Analytic many-body potential for GaAs(001) homoepitaxy: Bulk and surface properties

Kristen A. Fichthorn, Yogesh Tiwary, Thomas Hammerschmidt, Peter Kratzer, and Matthias Scheffler

Phys. Rev. B **83**, 195328 — Published 31 May 2011

DOI: 10.1103/PhysRevB.83.195328

An analytic many-body potential for GaAs(001) homoepitaxy: Bulk and surface properties

Kristen A. Fichthorn*

Departments of Chemical Engineering and Physics,

The Pennsylvania State University, University Park, PA 16802, USA

Yogesh Tiwary

Department of Chemical Engineering,

The Pennsylvania State University, University Park, PA 16802, USA

Thomas Hammerschmidt

Interdisciplinary Center for Advanced Materials Simulation,

Ruhr-Universität Bochum, Stiepeler Strasse 129, 44801 Bochum, Germany

Peter Kratzer

Faculty of Physics and CeNIDE, University Duisburg-Essen,

Lotharstrasse 1, 47048 Duisburg, Germany

Matthias Scheffler

Fritz-Haber-Institut der Max-Planck-Gesellschaft,

Faradayweg 4-6, D-14195 Berlin-Dahlem, Germany

Abstract

We employ atomic-scale simulation methods to investigate bulk and surface properties of an analytic Tersoff-Abell type potential for describing interatomic interactions in GaAs. The potential is a modified form of that proposed by Albe and colleagues[1], in which the cut-off parameters for the As-As interaction have been shortened. With this modification, many bulk properties predicted by the potential for solid GaAs are the same as those in the original potential, but properties of the GaAs(001) surface better match results from first-principles calculations with density-functional theory (DFT). We tested the ability of the potential to reproduce the phonon dispersion and heat capacity of bulk solid GaAs by comparing it to experiment and the overall agreement is good. In the modified potential, the GaAs(001) $\beta 2(2 \times 4)$ reconstruction is favored under As-rich growth conditions in agreement with DFT calculations. Additionally, the binding energies and diffusion barriers for a Ga adatom on the $\beta 2(2 \times 4)$ reconstruction generally match results from DFT calculations. These studies indicate that the potential is suitable for investigating aspects of GaAs(001) homoepitaxy.

I. INTRODUCTION

GaAs thin films are widely used for a variety of applications involving electronic devices, such as metal-semiconductor field-effect transistors (MESFETs)[2–4], optoelectronic devices, including lasers, light-emitting diodes, and solar cells[5–11], and spintronic devices[12,13]. The successful fabrication of these devices depends sensitively on the structure of the GaAs surface. GaAs thin films are often grown by molecular beam epitaxy (MBE), in which elemental sources of gallium and arsenic are heated so that they evaporate to provide Ga atoms and As dimers and tetramers that subsequently deposit onto a substrate. In principle, this allows for precise control of the composition and thickness of the growing surface. However, the lack of quantitative knowledge regarding the relationship between MBE growth conditions and the atomic-scale processes that determine film structure has hampered progress in achieving such precise control.

As an example, we consider GaAs(001) homoepitaxy. The GaAs(001) surface figures prominently in a number of GaAs thin-film applications and has been the subject of many studies, as is discussed in some recent reviews[14–16]. In typical MBE growth settings for homoepitaxy, the GaAs(001) substrate exhibits the As-rich $\beta2(2\times4)$ surface reconstruction[15,16]. Although the structure of the $\beta2(2\times4)$ unit cell has been well established experimentally[17–24] and theoretically[25–29], Pashley and colleagues have pointed out that the two-fold structural degeneracy of the $\beta2(2\times4)$ *unit cell* can lead to $\beta2(2\times4)$ *surfaces* that have a long-range disorder associated with occupancy of out-of-phase unit cells[24,30]. Their work indicates that the disordered surface is the real template on which growth occurs and that effects associated with surface disorder may play a significant role in governing growth kinetics[30]. To date, there is no quantitative growth model that includes such effects.

In terms of modeling growth, first-principles calculations can indicate energetically favored surface structures, as well as the energy barriers associated with kinetic events. However, these calculations are computationally expensive and limited to fairly small systems. A suitable semi-empirical potential would allow for molecular-dynamics (MD) or accelerated MD[31–33] simulations, as well as for extensive studies of surface structures and kinetic events, that could enable long-time kinetic Monte Carlo[34] simulations of growth. In this paper, we provide a brief review of currently existing semi-empirical potentials for GaAs and discuss their suitability for accurately modeling key surfaces in GaAs(001) homoepitaxy. We show

that with a slight modification of its parameters, the Tersoff potential proposed by Albe *et al.*[1] can stabilize the GaAs(001) $\beta 2(2 \times 4)$ reconstruction under appropriate As-rich growth conditions, while retaining a good description of many bulk properties of GaAs. We discuss the suitability of this potential for describing the binding and diffusion of a gallium atom on the GaAs(001) $\beta 2(2 \times 4)$ reconstruction.

II. SEMI-EMPIRICAL POTENTIALS FOR GAAS

A versatile semi-empirical potential for GaAs should be able to describe pure gallium and pure arsenic, which have semi-metallic behavior with mixed covalent and metallic bonding, as well as the compound semiconductor, whose bonds are largely covalent. To describe the complex and varied surface reconstructions of GaAs, charge redistribution among the surface bonds must be taken into account to satisfy electron counting requirements[35–37]. Accurately describing these different features is a challenge. Two-body potentials cannot capture the open structure of bulk compound semiconductors and three-body or higher-order terms are needed. Perhaps the first semi-empirical potential with three-body terms was that by Choi *et al.*[38], who combined a two-body Mie potential with a three-body Axilrod-Teller potential[38] to describe properties of bulk GaAs, as well as GaAs clusters. Murdick *et al.* later determined that this potential does not provide mechanical stability for the zinc blende structure of the bulk GaAs crystal[39]. Subsequent to these efforts, a number of different potentials have been developed, and major efforts can be broadly be classified as Tersoff-Abell type[40–42], Stillinger-Weber type[43], and bond-order type[44–47]. Here, we classify bond-order potentials as those which have been formally derived within the tight-binding model[45].

Significant efforts have been directed at developing semi-empirical potentials with similar forms to those suggested by Abell[40] and Tersoff[41,42], who take the approach of describing covalent interactions with pair potentials that are moderated by the local bonding environment via a three-body bond-order term. Khor and Das Sarma developed a Tersoff-like potential[48] and Ito, Khor, and Das Sarma parameterized this for GaAs[49]. Their potential is not smoothly continuous as the coordination changes, making it difficult to use in MD simulations. The earliest Tersoff potential for GaAs was developed by Smith[50]. Smith's parameters were fit to geometries and cohesive energies for small As, Ga and GaAs clusters, as well as to bulk cohesive energies. Sayed *et al.* modified Smith's form to improve the an-

gular dependence of the potential energy[51]; however, this parametrization does not correctly predict the lowest energy zinc blende phase of solid GaAs[52]. Conrad and Scheerschmidt[53] proposed a potential with the Tersoff form in which the bond-order term is based on the tight binding second-moment approximation. This potential gives an incorrect sign for the heat of formation of the GaAs zinc blende structure[1,39].

Albe *et al.*[1] parameterized a Tersoff potential by fitting to several structural parameters of bulk Ga, As and GaAs, including elastic moduli and bond lengths, as well as cohesive energies. This potential captures the correct ground-state structures of pure As and Ga, as well as the trends in the formation energies of point defects as compared to first principles calculations based on density-functional theory (DFT)[1]. In a review of the suitability of various potentials to describe GaAs(001) homoepitaxy, Murdick *et al.* concluded that Albe's version of the Tersoff potential is among the most promising[39]. Recently, Albe's potential has been used to study GaAs sputtering[54] and diffusion on the GaAs(001) surface[55]. Powell *et al.*[56] parameterized a Tersoff potential to accurately reproduce the elastic properties of bulk GaAs with a focus on matching Kleinman's internal displacement parameter. Unlike other parameterizations of the Tersoff potential[1,50,51,69], Powell's potential focuses only on Ga-As interactions, limiting its use to homogeneous bulk environments.

Stillinger-Weber[43] (SW) potentials, which contain both two- and three-body terms, have been developed for GaAs by two different research groups[57–59]. In a recent assessment of various potentials for MD simulation of GaAs(001) homoepitaxy, Murdick *et al.* concluded that the SW potential developed by Wang and Stroud[57] should not be used, and that the potential developed by Angelo and Mills[58] and Grein *et al.*[59] would work well only for Ga-As interactions, not elemental interactions[39]. This potential has been employed in MD simulation studies by Murdick, Zhou, and Wadley, who investigated atomic-scale processes relevant to the low-temperature growth of highly doped GaAs crystalline films[60].

One of the more recent descriptions for GaAs is a bond-order potential based on a tight-binding description of covalent bonding[61]. This potential contains 56 parameters that were set (or fitted) to match structural properties of Ga, As, and GaAs. Murdick and colleagues recently used this potential in MD simulations to study growth, as well as the adsorption, surface diffusion, and desorption of As_2 on GaAs(001) (1×2) and (2×1) surfaces[62].

A significant challenge for all semi-empirical GaAs potentials developed to date is describing its wide array of complex surface reconstructions that depend on the temperature,

pressure, and composition of the gas phase in equilibrium with the surface. Murdick and colleagues emphasized this point in their recent work[39,61,63], where they evaluated the capability of two different SW potentials[57,59], the Tersoff potential parameterized by Albe *et al.*[1], and their bond-order potential[61] to reproduce various GaAs(001) surface reconstructions that are predicted by DFT[64]. While DFT studies predict a progression from the $\zeta(4 \times 2)$ to the $\alpha 2(2 \times 4)$ to the $\beta 2(2 \times 4)$ to the $c(4 \times 4)$ reconstruction as the surface environment moves from Ga-rich to As-rich conditions[64], all of the potentials tested predict that the most stable surfaces are the (1×2) reconstruction under Ga-rich conditions and the (2×1) reconstruction under As-rich conditions[39,61,63]. As was discussed by Farrell[35] and Pashley[36], the reconstructions of GaAs surfaces can be understood in terms of an electron counting model in which the lowest energy structure is obtained with filled (low energy) As dangling bonds and empty (high energy) Ga dangling bonds. The electron redistribution among surface-atom bonds and dangling bonds that is necessary to minimize the surface energy is naturally incorporated in DFT calculations. The semi-empirical potentials, however, do not include this feature.

To account for electron redistribution between dangling bonds and surface-atom bonds at GaAs surfaces, Zhou and co-workers developed an electron counting potential[37]. This potential provides an additional term – the "electron counting term" – to existing potentials and it is nonzero only for atoms at the surface, so that the bulk properties predicted by these potentials are unaffected. When the electron counting potential is applied in conjunction with SW[57,59], Tersoff[1], and bond-order[61] potentials, their agreement with DFT improves substantially and they are able to predict that α and β reconstructions, similar to those predicted in DFT studies[64], are energetically preferred in the approximate range of chemical potentials where DFT predicts them to be preferred[47]. In the case of the bond-order potential, the additional electron counting potential even stabilizes the $c(4 \times 4)$ reconstruction under the most As-rich conditions[47,61], in agreement with DFT[64].

The large number of interatomic potentials developed for GaAs[1,38,49–51,53,56–59,61,65–69], which exceeds the number reviewed above, attests to the difficulty of accurately describing a wide range of physical properties within a single potential. As discussed above, this difficulty seems especially prevalent at surfaces. In this paper, we present a Tersoff potential that is a modified version of Albe's form[1] to provide a suitable means for studying GaAs(001) homoepitaxy on the $\beta 2(2 \times 4)$ reconstruction. We note that some of us[69] recently parame-

terized a Tersoff potential for GaAs and InAs, with a focus on surface properties. However, due to the reported problems in the parametrization of this potential[70], the potential of Albe *et al.* provides a generally better agreement with DFT results for surface energies of the reconstructions of the (001) surface, which is the subject of this work. We demonstrate that this potential can provide a reasonable description of many bulk properties, in addition to rendering the GaAs(001)$\beta 2(2\times 4)$ reconstruction stable under As-rich growth conditions and providing a good description of Ga adatom binding and surface diffusion compared to DFT calculations.

III. POTENTIAL MODEL

In the Tersoff potential, a solid containing N atoms with a configuration given by $\mathbf{R} = \{\mathbf{r_1}, \mathbf{r_2}, \ldots, \mathbf{r_N}\}$ has a potential energy $V(\mathbf{R})$ that is given by

$$V\left(\mathbf{R}\right) = \frac{1}{2}\sum_{i,j\neq i} f_{ij}^{c}\left(r_{ij}\right)\cdot\left[V_{ij}^{R}\left(r_{ij}\right) - B_{ij}\left(r_{ij}\right)\cdot V_{ij}^{A}\left(r_{ij}\right)\right] \quad . \tag{1}$$

Here, the sum runs over all atom pairs i and j, separated by a distance r_{ij}. The Tersoff potential consists of pair repulsive (V_{ij}^{R}) and attractive (V_{ij}^{A}) terms, as well as a three-body term (B_{ij}), which moderates the attractive term, playing the role of the bond order. The bond-order term is used to capture the effect that as the number of neighbors an atom has increases, the strength of the bonds to the neighbors decreases[41]. The form of the bond-order term was chosen such that the energy per bond is a monotonically decreasing function of coordination[41]. A short-ranged cutoff f_{ij}^{c} is used so that the forces smoothly go to zero at the first neighbor shell of the structure of interest. The repulsive and attractive terms are given by Morse potentials, with the form

$$V_{ij}^{R}\left(r_{ij}\right) = \frac{D_{ij}}{S_{ij}-1}\cdot\exp\left[-\beta_{ij}\sqrt{2S_{ij}}\left(r_{ij}-R_{ij}^{0}\right)\right] \quad , \tag{2}$$

and

$$V_{ij}^{A}\left(r_{ij}\right) = \frac{S_{ij}D_{ij}}{S_{ij}-1}\cdot\exp\left[-\beta_{ij}\sqrt{\frac{2}{S_{ij}}}\left(r_{ij}-R_{ij}^{0}\right)\right] \quad . \tag{3}$$

The bond-order term is given by

$$B_{ij}\left(r_{ij}\right) = \left[1+\left(\gamma_{ij}\cdot\chi_{ij}\left(r_{ij}\right)\right)\right]^{-\frac{1}{2}} \quad , \tag{4}$$

where

$$\chi_{ij}\left(r_{ij}\right)=\sum_{k\neq i,j} f_{ik}^{c}\left(r_{ik}\right)\cdot g_{ik}\left(\theta_{ijk}\right)\cdot\exp\left[\left(\alpha_{ik}\left(r_{ij}-r_{ik}\right)\right)\right] \quad , \tag{5}$$

and

$$g_{ik}\left(\theta_{ijk}\right)=\delta_{ik}\left(1+\frac{c_{ik}^{2}}{d_{ik}^{2}}-\frac{c_{ik}^{2}}{d_{ik}^{2}+\left(h_{ik}-\cos\theta_{ijk}\right)^{2}}\right) \quad . \tag{6}$$

The cutoff function has the form,

$$f_{ij}^{c}\left(r_{ij}\right)=\begin{cases}1 & r_{ij}-R_{ij}^{c}\leq -D_{ij}^{c}\\ \frac{1}{2}\left[1-\sin\left(\pi\frac{r_{ij}-R_{ij}^{c}}{2D_{ij}^{c}}\right)\right] & \left|r_{ij}-R_{ij}^{c}\right|<D_{ij}^{c}\\ 0 & r_{ij}-R_{ij}^{c}\geq D_{ij}^{c}\end{cases} \quad . \tag{7}$$

Most of the parameters for this potential have been published previously[1] and are shown in Table I for completeness.

For this work, we modify the As-As interaction by changing the two adjustable parameters in Eq. (7): We decrease R_{ij}^{c} from Albe's original value of 3.4 Å to 3.1 Å and we similarly decrease D_{ij}^{c} from 0.2 Å to 0.1 Å. Decreasing the cutoff shortens the As dimer length to 3.01 Å, which is closer to the DFT value of 2.5 Å than Albe's original value of 3.21 Å. As we will discuss below, the shorter cut-off parameters stabilize important GaAs(001) surface reconstructions without seriously compromising properties of bulk GaAs. This is because bulk properties, such as the GaAs bulk modulus and elastic constants depend only on the Ga-As potential: In a perfect, zinc-blende, bulk GaAs crystal, Ga-Ga and As-As bond lengths fall outside the cut-off distances listed in Table I and for Albe's original potential[1]. Thus, this modification of the potential retains the excellent agreement between Albe's original potential, first-principles calculations, and experiment for many bulk properties[1].

IV. BULK PROPERTIES

As discussed above, Albe's potential provides an excellent description of many bulk properties of GaAs[1] and the modified form should retain many of these properties. Below, we present tests of the potential for several additional bulk properties of solid GaAs.

TABLE I. Modified parameters from Albe *et al.*[1]

	Ga-Ga	As-As	Ga-As
δ_{ij}	0.007874	0.455	0.0166
S_{ij}	1.11	1.86	1.1417
β_{ij} (Å^{-1})	1.08	1.435	1.5228
D_{ij} (eV)	1.40	3.96	2.10
R^o_{ij} (Å)	2.3235	2.10	2.35
c_{ij}	1.918	0.1186	1.29
d_{ij}	0.75	0.1612	0.56
$h_{ij} = cos(\theta_{ijk})$	0.3013	0.07748	0.237
α_{ij} (Å^{-1})	1.846	3.161	0.0
R^c_{ij} (Å)	2.95	3.1	3.1
D^c_{ij} (Å)	0.15	0.1	0.2
γ_{ij}	1.0	1.0	1.0

A. Phonons

The vibrational properties predicted by the potential are characterized by the normal-mode frequencies and the phonon dispersion. We obtain the normal-mode frequencies from the dynamical matrix $\mathbf{D}$ with elements given by[71]

$$D_{i\alpha j\beta} = \frac{1}{\sqrt{m_i m_j}} \frac{\partial^2 V}{\partial r_{i\alpha} \partial r_{j\beta}} \quad , \tag{8}$$

where V is the potential energy, $m_{i(j)}$ is the mass of atom $i(j)$, and α and β represent the x, y, and z directions. For N atoms, $\mathbf{D}$ has dimensions of $(3N \times 3N)$ and the $3N-6$ nonzero eigenvalues $\{\lambda_i\}$ of $\mathbf{D}$ yield the normal-mode frequencies $\{\omega_i\}$ through $\omega_i = \lambda_i^{1/2}$. To obtain the dynamical matrix, we first relaxed the unit cell in a bulk crystal. This yielded a lattice constant of 5.653 Å, which closely matches the experimental value of 5.654 Å[72]. We then calculated elements of $\mathbf{D}$ for a bulk crystal consisting of 128 atoms with this lattice constant using finite (central) differences with atom displacements of ± 0.01 Å.

By solving the eigenvalue equation $\mathbf{D}(\mathbf{k}) \cdot \mathbf{u} = \lambda^2 \mathbf{u}$, we obtain the phonon dispersion.

Here, the elements of $\mathbf{D}(\mathbf{k})$ for a wave-vector $\mathbf{k}$ are given by[71]

$$D_{i\alpha,j\beta}\left(\mathbf{k}\right) = \sum_{n} \exp\left(-i\mathbf{k}\cdot\mathbf{R}_n\right) \frac{1}{\sqrt{m_i m_j}} \frac{\partial^2 V}{\partial r_{ni\alpha} \partial r_{0j\beta}} \quad . \tag{9}$$

In this equation, $\mathbf{R}_n$ are the Bravais lattice vectors of the N_p primitive unit cells comprising the crystal and the additional index on the terms comprising the dynamical matrix compared to Eq. (8) denotes unit cell $n(0)$. For our system, $\mathbf{D}(\mathbf{k})$ is a (6×6) matrix with six eigenvalues for all $\mathbf{k}$ in the first Brillouin zone. We used the PHON code[73], version 1.2, to calculate the phonon dispersion. Input to PHON consists of the forces on all the atoms in the supercell for two off-symmetry displacements suggested by PHON, one each for Ga and As. These are then used to generate the full force field. The resulting phonon dispersion is shown in Fig. 1.

Using inelastic neutron scattering at 12 K, Strauch and Dorner obtained experimental phonon dispersion curves for GaAs[74]. Giannozzi *et al.* used DFT calculations within the local density approximation (LDA) to determine these and their results match those of Strauch and Dorner almost exactly[75]. The experimental results are shown along with ours in Fig. 1. Here, we see that the potential captures the general shape and magnitude of the acoustic frequencies. The agreement between the potential and experiment is very good for the acoustic frequencies around $\mathbf{\Gamma}$, as is expected[76], since the potential provides a good description of the elastic constants[1]. The potential best captures the LA frequencies on the line between $\mathbf{\Gamma}$ and $\mathbf{X}$ – although it predicts higher frequencies than experiment for all the acoustic modes between $\mathbf{\Gamma}-\mathbf{K}-\mathbf{X}$. A similar trend is seen in a study of the phonon dispersion of GaAs by Powell and colleagues[77], who compared the phonon dispersions from a Tersoff potential with the parameters of Sayed *et al.*[51] to those from two different Tersoff potentials: one with parameters fit to reproduce elastic constants and one fit to the phonon dispersion. Powell *et al.* noted that it is difficult to find a parameter set that captures both the phonon frequencies and the elastic constants, as there is a trade off in accuracy between them[77]. The largest discrepancy between the potential and experiments for the acoustic frequencies is for the TA modes, which are overestimated by the potential.

The potential predicts higher frequencies for the optical modes compared to the experimental[74] data and there is no splitting of the optical frequencies at $\mathbf{\Gamma}$. The latter is a well-known consequence of the fact that the Tersoff-Abell potential does not include long-range electrostatic interactions of the cations and anions. Generally, the potential predicts higher phonon

frequencies than experiment. As we will see below, this will lead to an underestimation of the heat capacity[79].

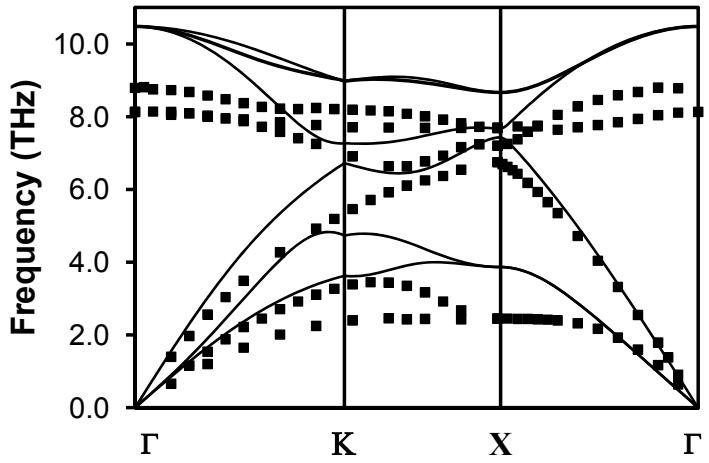

FIG. 1. Phonon dispersion for bulk GaAs. The lines are the phonon modes computed with the Tersoff potential in this work. Experimental results[74] are shown with squares.

We now turn to the thermal properties of bulk GaAs. In classical MD simulations, quantum effects are omitted that can become important at low temperatures. To include a correction for the zero-point energy in the MD simulations, we followed the procedure of Wang, Chan, and Ho[80,81]. In this method, the kinetic energy of the classical MD system is equated to the vibrational and zero-point energy of a quantum system to provide a temperature re-scaling given by

$$3\left(N-1\right)k_{\mathrm{B}}T_{\mathrm{MD}}=\frac{1}{2}\sum_{i}\hbar\omega_{i}+\sum_{i}\frac{\hbar\omega_{i}}{\left[\exp\left(\frac{\hbar\omega_{i}}{k_{\mathrm{B}}T_{\mathrm{real}}}\right)\right]-1} \quad , \tag{10}$$

where N is the number of atoms in the system, k_{B} is Boltzmann's constant, $\hbar$ is Planck's constant h divided by 2π, ω_i are the normal-mode frequencies, T_{MD} is the temperature used in the MD simulation, and T_{real} is the corrected temperature for zero-point vibration. As discussed above, we found the normal-mode frequencies from the eigenvalues of the dynamical matrix $\mathbf{D}$, whose elements are given by Eq. (8). Using Eq. (10), we found a relationship between T_{real} and T_{MD}. The resulting curve is plotted in Fig. 2. We note that

the curve in Fig. 2 can be fit by a polynomial of the form

$$T_{MD} = 156.73 - (0.050504)T_{real} + (0.0033433)T_{real}^2 - (5.2643 \times 10^{-6})T_{real}^3 + (3.9471 \times 10^{-9})T_{real}^4 - (1.1214 \times 10^{-12})T_{real}^5 \quad . \tag{11}$$

Equation (11) implies that the zero-point temperature of the MD system is ∼157 K: In a classical MD simulation with a temperature of 157 K, the actual temperature is 0 K. At 450 K, the real and MD temperatures are within 5% of one another and we reach the classical limit, where the temperature of the MD system is approximately equal to the temperature of the quantum system.

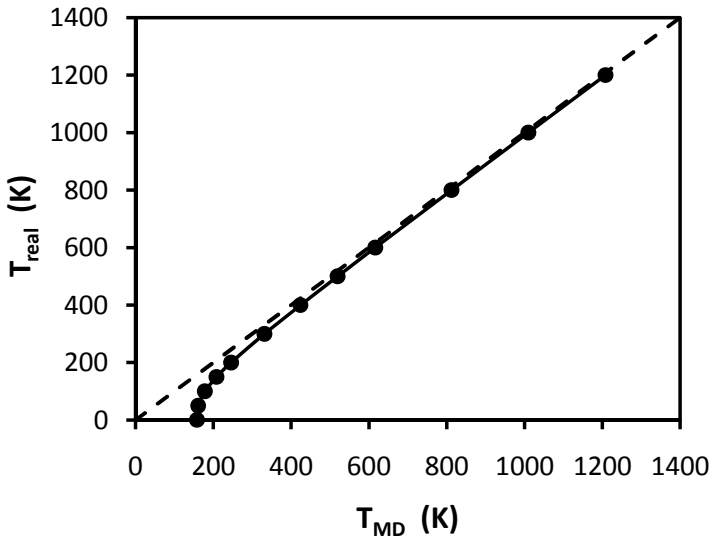

FIG. 2. The real temperature corrected for zero-point vibration (symbols), along with the polynomial fit in Eq. (11), as a function of the MD simulation temperature. The dashed line shows the classical result, in which $T_{real} = T_{MD}$.

B. Heat Capacity

We calculated the constant-volume heat capacity C_v, which is defined as

$$C_v = \left(\frac{\partial U}{\partial T}\right)_V \quad , \tag{12}$$

where U is the total energy. To obtain C_v, we used canonical-ensemble (NVT) MD, in which the number of particles N, box volume V, and temperature T are held constant. To

probe a range of densities relevant to experiment, we ran simulations with 1000 Ga and As atoms initially in the zinc-blende structure at two different densities (lattice constants): the density implied by the zero-temperature lattice constant predicted by the potential ($a = 5.65\mathring{A}$) and the liquid density ($a = 5.52\mathring{A}$). The Berendsen thermostat[82] was used to control the temperature because of its ease of use. Although the Berendesn thermostat does not guarantee the canonical ensemble, the errors are small for a sufficiently large system. For each temperature at a fixed density, we equilibrated the system for 250 ps. Ten subsequent production runs, each for 250 ps, were used to obtain the average energy U. We fitted the average energy as a function of the real temperature [*i.e.*, T_{real} given in Eq. (11)] using cubic spline interpolation in Mathematica[83] and took the derivative in Eq. (12) to obtain C_v. We can also obtain C_v using the harmonic approximation, which gives

$$C_{v,h}(T) = k_B \sum_i \frac{(\hbar\omega_i/k_BT)^2 \exp(\hbar\omega_i/k_BT)}{[\exp(\hbar\omega_i/k_BT) - 1]^2} \quad . \tag{13}$$

In the high-temperature limit, Eq. (13) reaches the constant Dulong-Petit value, in which C_v is equal to $3k_B$ per species in the primitive unit cell[84].

The results from the MD simulations and Eq. (13) are shown in Fig. 3 along with two sets of experimental results. In experiment, the constant-pressure heat capacity C_p is measured – although we expect C_p and C_v to be close for solid GaAs. The first set of experimental values for C_p were compiled by Adachi[85], who used data from the work of Cetas *et al.*[86], Piesbergen[87], Lichter and Sommelet[88], and Blakemore[89]. More recently, Glazov and Pashinkin[90] reevaluated the high-temperature data ($T \gtrsim 700$ K) of Lichter and Sommelet[88] and concluded that the data of Itagaki and Yamaguchi[92] is likely to be more accurate. They measured new values of C_p for T between 350 and 710 K and they fit their values of C_p, as well as selected literature values, to the Mayer-Kelly form for the temperature range between 200 and 1514 K[90]. Selected points from this fit are also shown in Fig. 3.

In Fig. 3, we see that there is overall good qualitative agreement between MD results and experiment. It should be noted that the temperature re-scaling in Eq. (10) is necessary to achieve even qualitative agreement between simulation and experiment at low temperatures. In quantitative terms, the MD simulations predict lower values of C_v than experiment for most temperatures. Over the low-temperature range ($T < 200$ K), the MD values of C_v agree well with the harmonic approximation in Eq. (13). Here, both MD and Eq. (13) predict values lower than experiment due to the tendency of the potential to predict the

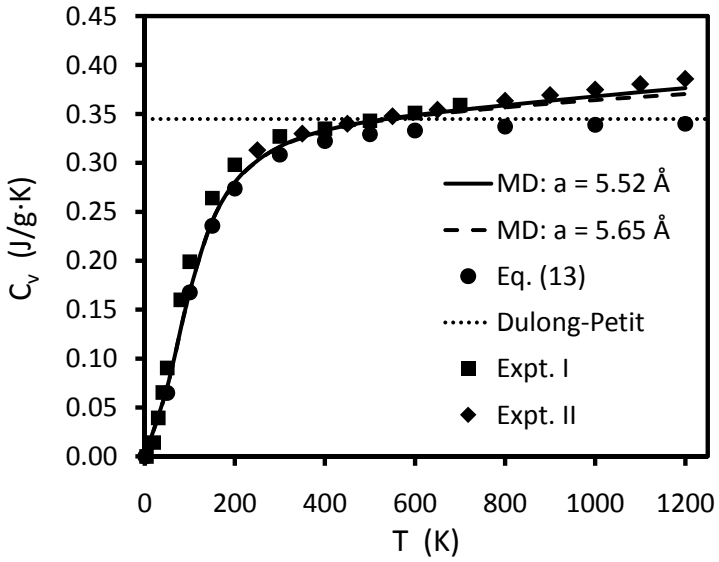

FIG. 3. Heat capacities as a function of temperature. Experimental results are taken from Adachi[85] (Expt. I) and Glazov and Pashinkin[90] (Expt. II).

phonon frequencies that are high compared to experiment (cf., Fig. 1). There is near-perfect agreement between MD simulations and experiment for temperatures between 400-800 K and the agreement worsens again higher temperatures. As the temperature approaches 1200 K, Eq. (13) approaches the Dulong-Petit limit. Deviations from Dulong-Petit behavior can be attributed to anharmonic effects, which are present in both the MD simulations and experiment, as well as to defects in the bulk crystals in the experiments[84]. Interestingly, the values of C_v from MD simulations at both lattice constants are in nearly perfect agreement at low and intermediate temperatures. At the highest temperatures, around 1200 K, the deviation between the two values of C_v is the greatest ($\sim 2\%$) and the values of the heat capacity associated with the smaller (liquid) lattice constant are in better agreement with experiment.

V. SURFACE PROPERTIES

A. GaAs(001) Surface Energies

To determine the suitability of this potential to describe the surfaces important for GaAs(001) homoepitaxy, we calculated a phase diagram of surface free energies for vari-

ous GaAs(001) reconstructions. The surface free energy γ of a symmetric slab with two identical free surfaces is given by

$$\gamma = \frac{1}{2A}\left[U_{slab}^{tot} - N_{Ga}E_{GaAs}^{bulk} - (N_{As} - N_{Ga})\,\mu_{As}\right] \quad , \tag{14}$$

where U_{slab}^{tot} is the total energy of the slab, A is the surface area, E_{GaAs}^{bulk} is the bulk cohesive energy per GaAs pair of zinc blende GaAs, N_i is the number of atoms of species i, and μ_{As} is the chemical potential of As. The factor of two is needed to take into account the double-sided slab used to obtain U_{slab}^{tot}. From the potential, $E_{GaAs}^{bulk} = -6.71$ eV/GaAs pair for a relaxed bulk crystal at 0 K[1]. The As chemical potential is a variable in Eq. (14) and it must be large enough to ensure that As would not evaporate from the surface to leave pure Ga behind and small enough to prevent crystalline As from forming on the surface. These considerations provide the bounds

$$\Delta H_f < \mu_{As} - \mu_{As}^{bulk} < 0 \quad , \tag{15}$$

where $\Delta H_f = E_{GaAs}^{bulk} - E_{Ga}^{bulk} - E_{As}^{bulk}$ is the heat of formation of GaAs. We obtained $\Delta H_f = -0.912$ eV/GaAs pair from the potential and $E_{As}^{bulk} = \mu_{As}^{bulk} =$ -2.965 eV/GaAs pair for the lowest-energy phase of As (αAs) at 0 K. The lowest-energy phase was obtained from conjugate gradient minimizations, such that the force on any given atom was below 1 meV/Å. We note that this is the same value given by Albe[1] for the original potential, but it is different than the value of μ_{As}^{bulk} that Murdick *et al.* found using Albe's potential[63] for αAs. We computed U_{slab}^{tot} for the various surface reconstructions indicated in Figs. 4 and 5. In these calculations, two surfaces are separated by 15 layers of bulk GaAs. A full layer consists of 64 atoms. Beginning with atoms in configurations similar to those predicted by DFT with the generalized-gradient approximation (GGA) PBE exchange-correlation functional[64], we used the conjugate gradient method to minimize the surface energy. The surface energies as a function of $\mu_{As} - \mu_{As}^{bulk}$ are shown in Fig. 5(a). Lee, Moritz, and Scheffler used DFT with the GGA-PBE functional to study these reconstructions[64] and their results are shown in Fig. 5(b). DFT within the LDA gives a very similar energetic hierarchy of surface reconstructions, but the absolute values of surface energies in LDA are generally larger (cf., Ref 26), and thus closer to the values obtained with our potential.

The surface energies in Fig. 5 have also been probed by Murdick and colleagues[39,61,63] for various semi-empirical potentials[1,57,59,61]. They found that all of the potentials tested

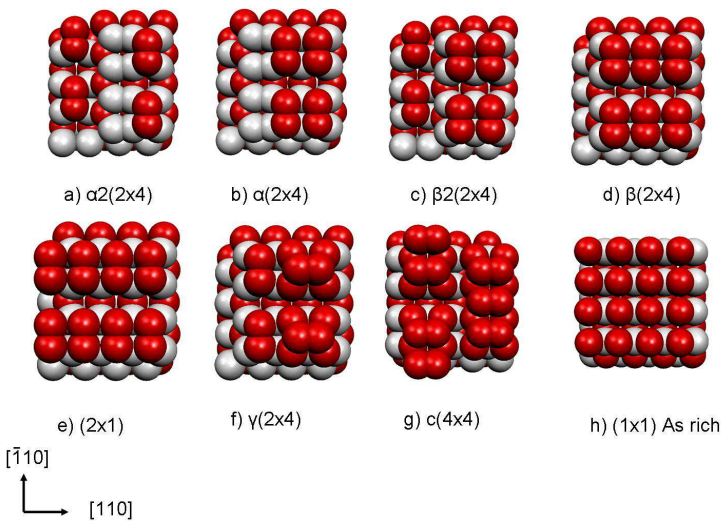

FIG. 4. (Color online) Top down view of the As-rich surfaces used in the surface free-energy calculations. As atoms are shown in red (dark) and Ga atoms are shown in white.

predict the most stable surfaces to be the (1×2) reconstruction under Ga-rich conditions and the (2×1) reconstruction under As-rich conditions[39,61,63]. Similar to Murdick and colleagues, we find the Ga-rich (1×2) reconstruction to be the most favored surface at low As chemical potentials. However, we find that the $\beta(2\times4)$ and the $\beta2(2\times4)$ reconstructions are favored under As-rich conditions. These reconstructions are shown in Fig. 4(c) and (d). The $\beta2(2 \times 4)$ reconstruction consists of rows of As-dimer pairs separated by trenches with lone As dimers, whereas the $\beta(2 \times 4)$ reconstruction has rows that are three As dimers in width separated by trenches without As dimers. In our calculations, the β reconstruction is energetically favored over the $\beta2$ by less than 2 meV/ Å^2. DFT calculations[64,91] have shown that the β is several meV/ Å^2 higher in energy than the $\beta2$ due to electrostatic interactions not captured by the potential. Between the (1×2) reconstruction at low μ_{As} and the $\beta/\beta2(2 \times 4)$ reconstructions at high μ_{As}, there is an intermediate region where we predict that the $\beta(4 \times 2)$ and the $\beta2(4 \times 2)$ reconstructions are preferred.

Interestingly, we find that the As-rich (2×1) reconstruction [cf., Fig. 4(e)], which was found to be energetically preferred under As-rich conditions by Murdick and colleagues for other empirical potentials[39,61,63], has a high energy that is off the scale in Fig. 5(a). Although there is an energetic gain from the formation of As dimers on the (2×1) surface, these dimers (with their short separation compared to that in Albe's original potential[1]) pull

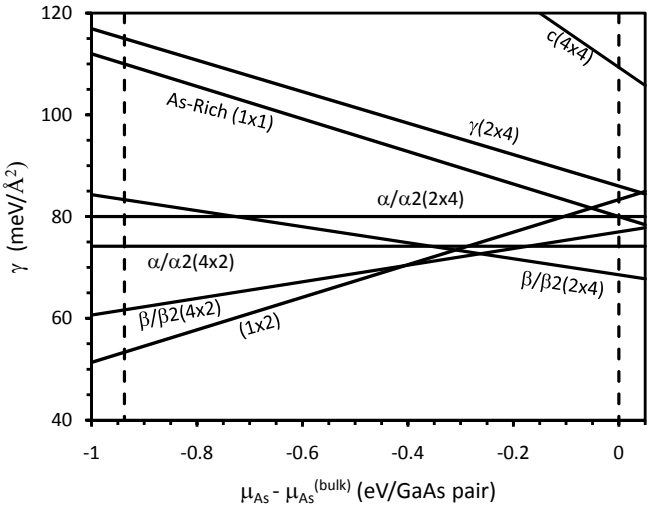

(a)

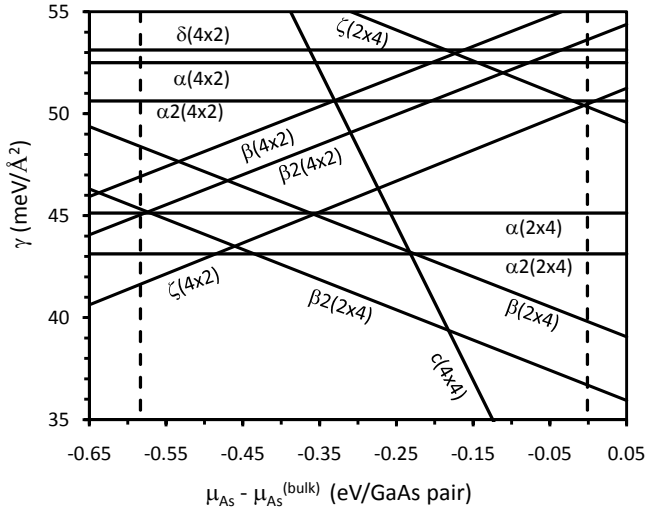

(b)

FIG. 5. Surface free-energy diagram for various possible reconstructions of the GaAs(001) surface for (a) the potential and; (b) DFT with the GGA-PBE exchange-correlation functional[64]. The dashed vertical lines represent the bounds in Eq. (15). Reconstructions with energies less than 3 meV/ Å^2 apart have been shown with one line.

the second-layer Ga atoms away from the third-layer As atoms, straining the Ga-As bonds. For each As dimer formed in the (2×1) reconstruction, four Ga-As bonds are stretched $\sim$0.1 Å away from their preferred bulk distance. In the $\beta/\beta2(2\times4)$ reconstructions, this strain is relieved for second-layer Ga-atom pairs that border the trenches. Thus, the bonds formed

by these second-layer Ga atoms and their third-layer As neighbors are closer to the preferred bulk distance. It is worth mentioning that we performed preliminary MD simulations of the $\beta 2(2\times4)$ reconstruction over temperatures ranging from 300 - 900 K and over times covering several ns. We found this reconstruction to be stable in all of these simulations.

Comparing the surface energies in Fig. 5(a) to results from DFT GGA-PBE calculations[64] in Fig. 5(b), we see that the potential is still far from matching DFT in the Ga-rich region. As seen in Fig. 5(b), DFT calculations predict that the $\zeta(4\times2)$ and the $\alpha2(2\times4)$ reconstructions are favored under Ga-rich conditions[64], instead of the Ga-rich (1×2) reconstruction that we see here. Although the DFT study predicts that the $\beta2(2\times4)$ reconstruction is favored under As-rich conditions (as we find), this study also predicts that the $c(4\times4)$ reconstruction is favored under the most As-rich conditions, in contrast to what we see here. Nevertheless, it is significant that the modified Tersoff potential predicts that the GaAs(001)$\beta2(2\times4)$ reconstruction is stable under As-rich conditions. This reconstruction occupies a large portion of the phase diagram established by Däweritz and Hey[93] for the GaAs(001) surface and it exists at the temperatures and As overpressures commonly found in GaAs homoepitaxial growth by MBE. Thus, in terms of its surface energy, the potential seems suitable for investigating atomic-scale processes in GaAs(001) homoepitaxy.

B. Ga Adatom Binding Sites on GaAs(001)$\beta2(2\times4)$

To assess the location and depth of binding sites for Ga adatoms, we calculated the minimum-potential-energy surface (MPES) for a Ga adatom on the $\beta2(2\times4)$ reconstruction. The MPES is a map of the minimum binding energy of a Ga adatom in a grid spanning the $\beta2(2\times4)$ unit cell. The binding energy E_b is given by

$$E_b = E_{s+a} - E_s \quad , \tag{16}$$

where E_{s+a} is the energy of a relaxed slab containing a Ga adatom and E_s is the energy of a bare, relaxed slab. We initially probed slabs ranging in thickness from seven to 12 layers and found that the differences in the binding energies for slabs thicker than seven layers were negligible. We chose to use a slab nine layers thick, consisting of 15 surface $\beta2(2\times4)$ unit cells, for a total of 990 atoms. The bottom three layers of atoms were fixed to the bulk coordinates and the rest of the layers were allowed to relax.

The starting positions for the adatom in the minimization were set by a grid in the surface plane with a 0.2 Å spacing in both the x and y ([110] and [$\bar{1}$10]) directions. At each point on the grid, a Ga adatom was placed above the surface beyond the potential cut-off distance, such that there was no interaction between the adatom and the surface. The adatom was then lowered in 0.1 Å increments in the z-direction until it was within the potential cut-off and we noted a change in the total energy. From this starting point, the adatom was further lowered closer to the surface. Three sets of maps were created by using initial positions 0.5, 1.0, and 1.5 Å closer than the cut-off distance. Conjugate-gradient minimization was used to relax the surface atoms, as well as the z coordinate of the adatom, until the maximum force on any single moving atom was below 0.001 eV/Å. The lowest-energy minima from all of the runs described above were used to create the total MPES map shown in Fig. 6. Table II summarizes the binding energies from our calculations, and compares them to results obtained with a similar methodology by Salmi *et al.*[96], who used a Tersoff potential with Sayed's parameters[51]. Many of the minima in Fig. 6 have also been seen in various DFT studies. Both LDA and GGA data with the PBE exchange-correlation functional for selected configurations have been published by Kratzer, Morgan, and Scheffler[95]. In order to complete this data set, we performed additional, hitherto unpublished GGA-PBE calculations on a coarse grid to map out the MPES. The results obtained with the same technical settings as described in Ref. 95 are given in Table II. Moreover, we compare to the DFT study of Kley, Ruggerone, and Scheffler[94], who calculated the MPES using the GGA with the PW-II exchange-correlation functional.

We first note that the only minimum in Table II that is seen in all the studies is the long-bridge site between two As trench dimers (E3), whose energy is taken as a reference to allow comparisons between the various results. Relative to E3, our calculations, DFT LDA calculations, and those of Salmi *et al.* predict the deepest minimum to be adjacent to an As trench dimer (E1a), while the deepest minimum in both DFT GGA calculations is one that breaks an As trench dimer (E1). E1 is the second-deepest minimum for us, as well as for the DFT LDA study, while the DFT GGA-PBE study puts E1a as second deepest. E1a is not seen in the DFT GGA PW-II study. Next in the energy ranking in our study and in the DFT studies is E2, for which we find good agreement with DFT GGA-PBE and LDA values. E2 is not seen in the study by Salmi *et al.*[96], who find that the binding site with next-lowest energy is E2a. The E2a site is similar to E1a, in that it flanks the short-bridge

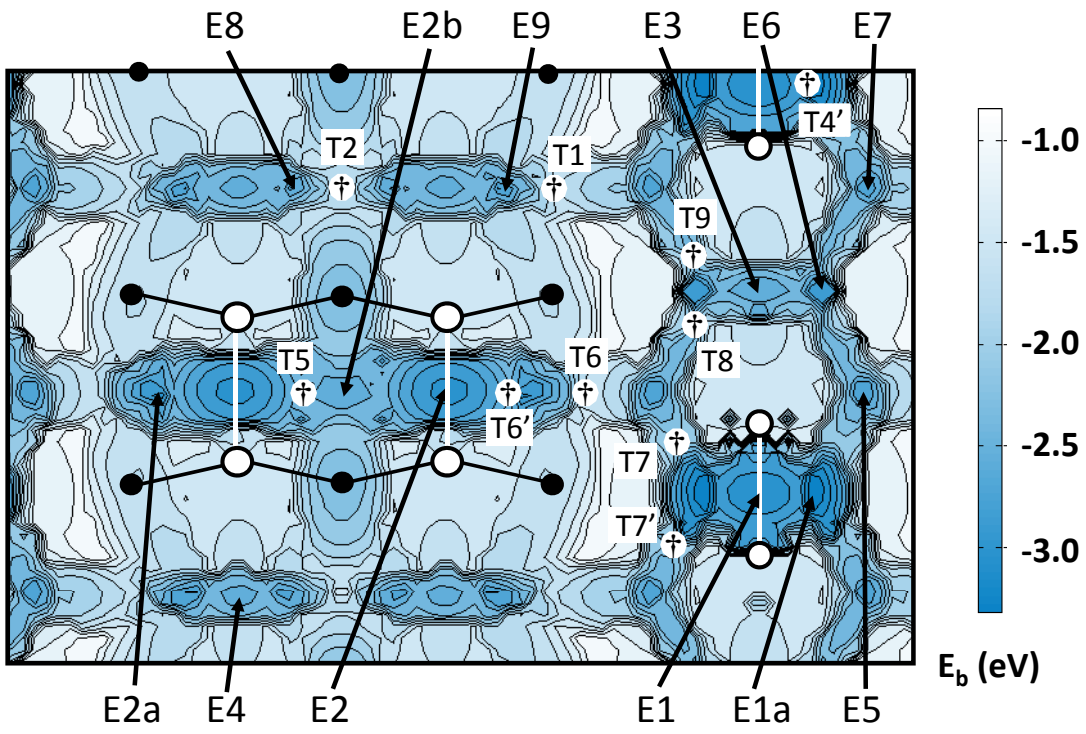

FIG. 6. (Color online) MPES of a gallium atom on the $\beta 2(2\times4)$ reconstruction. Key binding sites (energy minima) are labeled as E and transition states are indicated with † and labeled with T. Ga atoms are shown as black circles and As atoms are shown as white circles.

E2 site in the dimer row. This site is not seen (or mentioned) in the DFT studies. We found stable binding sites at both E2 and E2a, which have approximately equal energies. A related minimum that flanks the As-row dimers in the center of the row is E2b, which has the same binding energy in our study and in the DFT GGA-PBE study, but is not seen (or mentioned) in the other studies. There is good agreement among all studies that the long-bridge site between As dimers in the row (E4) is among the weakest minima.

Our potential predicts that the short-bridge binding sites between two As dimer atoms have similar energies, regardless of the location of the dimer, *i.e.* in the trench (E1) or in the row (E2). The energies of the long-bridge sites between two As dimers (E3 and E4) are also close, with a difference of 0.1 eV. This trend is seen in the LDA and the GGA-PBE results – although it differs from the DFT GGA PW-II calculations, which give one deep minimum between two As atoms in the trench (E1) and three similar minima elsewhere.

In addition to the minima discussed above, we find five other minima with comparable, but generally weaker energies. Two of these (E5 and E6) are also seen in the DFT GGA-PBE

TABLE II. Relative binding energies (in eV) for minima in Ga binding on the $\beta 2(2\times4)$ reconstruction indicated in Fig. 6. Results are shown for the potential used in this work, as well as for DFT studies with the GGA PW-II (Ref. 94), the GGA PBE (Ref. 95 plus unpublished work), and the LDA (Ref. 95). Additionally, we show results from Ref. 96 with a Tersoff potential parameterized with Sayed's parameters[51], denoted by P2. All binding energies [E_b from Eq. (16)] are given relative to the energy at the long-bridge site in the trench (E3), which is set to zero. The symbol $\emptyset$ signifies that the minimum is absent, while the entries marked — are unavailable.

site	this work	GGA PW-II	GGA PBE	LDA	P2
E1	−0.5	−0.7	−0.6	−0.4	$\emptyset$
E1a	−0.8	$\emptyset$	−0.4	−0.6	−0.9
E2	−0.4	−0.1	−0.4	−0.3	$\emptyset$
E2a	−0.4	$\emptyset$	$\emptyset$	—	−0.8
E2b	0.0	$\emptyset$	0.0	—	$\emptyset$
E3	0.0	0.0	0.0	0.0	0.0
E4	0.1	0.3	0.1	—	0.0
E5	−0.2	$\emptyset$	0.1	—	$\emptyset$
E6	−0.3	$\emptyset$	0.0	—	$\emptyset$
E7	−0.2	$\emptyset$	$\emptyset$	—	$\emptyset$
E8	−0.1	$\emptyset$	$\emptyset$	—	$\emptyset$
E9	−0.2	$\emptyset$	$\emptyset$	—	$\emptyset$

study, although we predict somewhat stronger binding than DFT. We note that E7 in our study is similar to E5 in its position relative to the As trench dimer, but its position relative to the row dimers is different. Nevertheless, we find that the difference in binding energies between E5 and E7 is less than 0.1 eV so these two sites might be taken as equivalent. The remaining minima that we find flank the long-bridge sites between As-row dimers (E8 and E9). These minima are not seen in the other studies and, while they may arise due to conceptual shortcomings of the potential, we note that the resolution of our MPES is finer than that in the DFT studies (0.2 Å vs. 1.0 Å) so it is possible that some of these minima would occur in a DFT study with finer resolution. It is also important to point

TABLE III. Transition-state energies (in eV) on the $\beta 2(2\times4)$ reconstruction. Transition-state energies are obtained from Eq. (16) and are given relative to the energy at the long-bridge site in the trench (E3), which is set to zero.

Transition State	T1	T2	T3	T4	T4'	T5	T6	T6'	T7	T7'	T8	T9
This Work	1.0	0.8	—	—	−0.2	0.2	0.9	0.1	0.5	0.4	0.3	0.3
GGA PW-II[94]	0.8	0.7	0.9	0.5	—	1.0	1.0	—	0.6	—	—	—
P2[96]	—	—	0.6	0.8	—	—	—	1.2	—	—	—	—

out that the relative Ga atom binding energies in these minima are significantly less than those of the deepest minima, so that they will be occupied infrequently at temperatures of interest. Overall, we find good agreement between the potential and DFT – especially LDA and GGA-PBE results – in the binding energies for a Ga adatom.

C. Ga Adatom Diffusion on GaAs(001) $\beta 2(2\times4)$

Another test of the potential to describe aspects of GaAs(001) homoepitaxy is to assess the energy barriers for a Ga atom to diffuse via hopping on the $\beta 2(2\times4)$ reconstruction. Diffusion-energy barriers are given by the energy difference between a transition state and an initial binding site. Transition states are first-order saddle points on the MPES and some relevant transition states can be found in Fig. 6. In analogous DFT GGA PW-II calculations[94], Kley, Ruggerone, and Scheffler identified seven different transition states. The potential reproduces most of these in similar locations to those in the DFT study and a comparison between the potential and DFT is shown in Table III. In Table III, we also include transition states found by Salmi *et al.*, who used a Tersoff potential parameterized with Sayed's parameters[51,96].

In Table III we see that most of our transition-state energies are in good agreement with DFT values and that we achieve better agreement with DFT than Salmi *et al.*[96]. One discrepancy occurs for T3: We find that a minimum (E2b) occurs at the location of T3 in the DFT GGA PW-II study. We note that the DFT GGA-PBE study also finds a minimum at E2b (T3)[95], so there is controversy at this location. In the DFT study, T3 (E2b) is co-linear and adjacent to T5[94]. Although we find a transition state in the vicinity of the

DFT T5, our agreement with DFT is poor. This may reflect inaccuracies of the potential at describing As dimer breaking, as this is required to proceed from E2 to the middle of the row. A similar issue occurs for T4 and T4'. In the DFT GGA PW-II study, T4 is located next to an unbroken As dimer[94], while we find that T4' corresponds to a broken dimer. We see that the energy of T4' is low, reflecting its location in the deep energy well surrounding the As trench dimer.

As for the binding sites, we find transition states that are not mentioned in the DFT GGA PW-II study. Two of these, T6' and T7' lie close to the DFT locations for T6 and T7. Actually, T6 in the DFT study lies near the minimum E2a in our study and is, thus, between T6 and T6' in our study. Similar to T4' and T5, T6' lies on the path from a broken to an unbroken As dimer and its energy is low. T6 in our study is associated with a transition between unbroken dimers and its value is reasonably close to the DFT value. A relatively minor issue arises with T7 and T7': In the DFT study, these two locations apparently have the same energy values, while we find a small difference of 0.1 eV, which might be expected due to the slightly different environments of these two locations. The other two transition states indicated in Fig. 6 and Table III are associated with transitions between E5 and E6 (T8) and E6 and E7 (T9). These transition states (and their associated minima) were not mentioned in the DFT GGA PW-II study, although the minima are seen in DFT GGA-PBE calculations (cf., Table II).

VI. CONCLUSIONS

In summary, we examined several bulk and surface properties of a Tersoff-Abell potential for GaAs that is a slightly modified form of Albe's potential[1]. We quantified the phonon dispersion and found that the modified potential captures the general shape of the experimentally observed acoustic-mode frequencies and describes some of them quantitatively, although overall it tends to predict higher frequencies than experiment for both the acoustic and optical modes. Using the phonon frequencies, we calculated a correction for classical MD simulation temperatures to account for the zero-point energy and we found that this was necessary to achieve good agreement between experimental and simulated heat capacities with classical MD.

Interestingly, the shorter As-As cut-off parameters in the modified potential greatly affect

the various reconstructions it predicts for the GaAs(001) surface. It is significant that the $\beta 2(2 \times 4)$ reconstruction is favored under As-rich growth conditions. This reconstruction exists at the temperatures and As overpressures commonly found in GaAs homoepitaxial growth by MBE. Additionally, we constructed a MPES for a Ga adatom on the $\beta 2(2 \times 4)$ reconstruction. Generally, we observe good agreement between the potential and DFT results regarding the locations of binding sites and transition states – although the potential predicts lower energies than DFT for transition states associated with dimer breaking/unbreaking moves. Nevertheless, our calculations indicate that energies and energy differences are similar between the potential and DFT, so that the potential provides a reasonable description of Ga adatom diffusion. Thus, our studies indicate that the potential is suitable for investigating aspects of GaAs(001) homoepitaxy.

VII. ACKNOWLEDGMENTS

This work was funded by the National Science Foundation, grant number DMR-1006452. We acknowledge helpful input from Maria Mignogna and Dr. Yangzheng Lin.

---

* E-mail: fichthorn@psu.edu

[1] K. Albe, K. Nordlund, J. Nord, and A. Kuronen, Phys. Rev. B **66**, 035205 (2002).

[2] M. Feng, P. J. Apostolakis, and W.-H. Chang, in *Properties of Gallium Arsenide, 3rd ed.*, edited by M. R.Brozel and G. E.Stillman (INSPEC, London,1996), Vol. 16, p. 785.

[3] L. E. Larson, IEEE J. of Solid-State Circuits **33**, 387 (1998).

[4] H. E. Katz, Electroanalysis **16**, 1837 (2004).

[5] P. K. Bhattachatya, in *Properties of Gallium Arsenide, 3rd ed.*, edited by M. R.Brozel and G. E.Stillman (INSPEC, London,1996), Vol. 16, p. 861.

[6] A. V. Krishnamoorthy and D. A. B. Miller, IEEE J. of Selected Topics in Quantum Electronics **2**, 55 (1996).

[7] G. Müller, P. Berwian, E. Buhrig, and B. Weinert, Topics Appl. Phys. **78**, 121 (2000).

[8] P. Bhattacharya, S. Ghosh, and A. D. Stiff-Roberts, Annu. Rev. Mater. Res. **34**, 1 (2004).

[9] L. L. Kazmerski, J. of Electron Spectroscopy and Related Phenomena **150**, 105 (2006).

[10] A. J. Shields, Nature Photonics **1**, 215 (2007).

[11] S. Mokkapati and C. Jagadish, Materialstoday **12**, 22 (2009).

[12] Y. Ohno, D. K. Young, B. Beschoten, F. Matsukura, H. Ohno, and D. D. Awschalom, Nature (London) **402**, 790 (1999).

[13] B. T. Jonker, Proc. IEEE **91**, 727 (2003).

[14] V. P. LaBella, M. R. Krause, Z. Ding, and P. M. Thibado, Surf. Sci. Rep. **60**, 1 (2005).

[15] A. Ohtake, Surf. Sci. Rep. **63**, 295 (2008).

[16] B. A. Joyce and D. D. Vvedensky, Mater. Sci. Eng. R **46**, 127 (2004).

[17] P. K. Larsen and D. J. Chadi, Phys. Rev. B **37**, 8282 (1988).

[18] A. Ichimiya, Y. Nishikawa, and M. Uchiyama, Surf. Sci. **493**, 232 (2001).

[19] J. M. McCoy, U. Korte, and P. A. Maksym, Surf. Sci. **418**, 273 (1998).

[20] A. Ohtake, M. Ozeki, T. Yasuda, and T. Hanada, Phys. Rev. B **65**, 165315 (2002).

[21] T. Hashizume, Q.-K. Xue, A. Ichimiya, and T. Sakurai, Phys. Rev. B **51**, 4200 (1995).

[22] Y. Garreau, M. Sauvage-Simkin, N. Jedrecy, R. Pinchaux, and M. B. Veron, Phys. Rev. B **54**, 17638 (1996).

[23] M. D. Pashley, K. W. Haberern, W. Friday, J. M. Woodall, and P. D. Kirchner, Phys. Rev. Lett. **60**, 2176 (1988).

[24] D. W. Pashley, J. H. Neave, and B. A. Joyce, Surf. Sci. **582**, 189 (2005).

[25] T. Ohno, Thin Solid Films **272**, 331 (1996).

[26] N. Moll, A. Kley, E. Pehlke and M. Scheffler, Phys. Rev. B **54**, 8844 (1996).

[27] S. B. Zhang and A. Zunger, Phys. Rev. B **53**, 1343 (1996).

[28] W. G. Schmidt and F. Bechstedt, Phys. Rev. B **54**, 16742 (1996).

[29] V. P. LaBella, H. Yang, D. W. Bullock, P. M. Thibado, P. Kratzer, and M. Scheffler, Phys. Rev. Lett. **83**, 2989 (1999).

[30] D. W. Pashley, J. H. Neave, and B. A. Joyce, Surf. Sci. **603**, L1 (2009).

[31] A. F. Voter, F. Montalenti, and T. C. Germann, Annu. Rev. Mater. Res. **32**, 321 (2002).

[32] R. A. Miron and K. A. Fichthorn, J. Chem. Phys. **119**, 6210 (2003).

[33] R. A. Miron and K. A. Fichthorn, Phys. Rev. Lett. **93**, 128301 (2004).

[34] K. A. Fichthorn and W. H. Weinberg, J. Chem. Phys. **95**, 1090 (1991).

[35] H. H. Farrell, J. P. Harbison, and L. D. Peterson, J. Vac. Sci. Technol. B **5**, 1482 (1987).

[36] M. D. Pashley, Phys. Rev. B **40**, 10481 (1989).

[37] X. W. Zhou, D. A. Murdick, and H. N. G. Wadley, J. Appl. Phys. **99**, 064908 (2006).

[38] D. K. Choi, S. M. Koch, T. Takai, T. Halicioglu, and W. A. Tiller, J. Vac. Sci. Technol. B **6**, 1140 (1988).

[39] D. A. Murdick, X. W. Zhou, and H. N. G. Wadley, Phys. Rev. B **72**, 205340 (2005).

[40] G. C. Abell, Phys. Rev. B **31**, 6184 (1985).

[41] J. Tersoff, Phys. Rev. B **37**, 6991 (1988).

[42] J. Tersoff, Phys. Rev. B **39**, 5566 (1989).

[43] F. H. Stillinger and T. A. Weber, Phys. Rev. B **31**, 5262 (1985).

[44] D. G. Pettifor, Phys. Rev. Lett. **63**, 2480 (1989).

[45] D. G. Pettifor and I. I. Oleinik, Phys. Rev. B **59**, 8487 (1999).

[46] D. G. Pettifor and I. I. Oleinik, Phys. Rev. B **65**, 172103 (2002).

[47] R. Drautz, X. W. Zhou, D. A. Murdick, B. Gillespie, H. N. G. Wadley, and D. G. Pettifor, Prog. Mater. Sci. **52**, 196 (2007).

[48] K. E. Khor and S. Das Sarma, Phys. Rev. B **38**, 3318 (1988).

[49] T. Ito, K. E. Khor, and S. Das Sarma, Phys. Rev. B **41**, 3893 (1990).

[50] R. Smith, Nucl. Instrum. Methods Phys. Res. B **67**, 335 (1992).

[51] M. Sayed, J. H. Jefferson, A. B. Walker, and A. G. Cullis, Nucl. Instrum. Methods Phys. Res. B **102**, 218 (1995).

[52] K. Nordlund and A. Kuronen, Nucl. Instrum. Methods Phys. Res. B **159**, 183 (1999).

[53] D. Conrad and K. Scheerschmidt, Phys. Rev. B **58**, 4538 (1998).

[54] E. Despiau-Pujo, P. Chabert, and D. B. Graves, J. Vac. Sci. Technol. A, **26**, 274 (2008).

[55] K. Li and B. Pan, Chin. J. Chem. Phys. **21**, 69 (2008).

[56] D. Powell, M. A. Migliorato, and A. G. Cullis, Phys. Rev. B **75**, 115202 (2007).

[57] Z. Q. Wang and D. Stroud, Phys. Rev. B **42**, 5353 (1990).

[58] J. E. Angelo and M. J. Mills, Philos. Mag. A **72**, 635 (1995).

[59] C. H. Grein, J. P. Faurie, V. Bousquet, E. Tourni, R. Benedek, and T. de la Rubia, J. Cryst. Growth **178**, 258 (1997).

[60] D. A. Murdick, X. W. Zhou, and H. N. G. Wadley, J. Cryst. Growth **286**, 197 (2006).

[61] D. A. Murdick, X. W. Zhou, H. N. G. Wadley, D. Nguyen-Manh, R. Drautz, and D. G. Pettifor, Phys. Rev. B **73**, 045206 (2006).

[62] D. A. Murdick, H. N. G. Wadley, and X. W. Zhou, Phys. Rev. B **75**, 125318 (2007).

[63] D. A. Murdick, X. W. Zhou, H. N. G. Wadley, and D. Nguyen-Manh, J. Phys.: Condens. Matter **17**, 6123 (2005).

[64] S.-H. Lee, W. Moritz, and M. Scheffler, Phys. Rev. Lett. **85**, 3890 (2000).

[65] M. Nakamura, H. Fujioka, K. Ono, M. Takeuchi, T. Mitsui, and M. Oshima, J. Cryst. Growth **209**, 232 (2000).

[66] X. Su, R. K. Kalia, A. Nakano, P. Vashishta, and A. Madhukar, J. App. Phys. **94**, 6762 (2003).

[67] J. Cai, X. Hu, and N. Chen, J. Phys. Chem. Solids **66**, 1256 (2005).

[68] J. T. Titantah, D. Lamoen, M. Schowalter, and A. Rosenauer, J. Appl. Phys. **101**, 123508 (2007).

[69] T. Hammerschmidt, P. Kratzer, and M. Scheffler, Phys. Rev. B **77**, 235303 (2008).

[70] T. Hammerschmidt, P. Kratzer, and M. Scheffler Phys. Rev. B **81**, 159905(E) (2010).

[71] E. Kaxiras, *Atomic and Electronic Structure of Solids* (Cambridge University Press, Cambridge 2003).

[72] J. C. Brice, in *Properties of Gallium Arsenide, 3rd ed.*, edited by M. R.Brozel and G. E.Stillman (INSPEC, London,1996).

[73] D. Alfè, Comp. Phys. Comm. **180**,2622 (2009).

[74] D. Strauch and B. Dorner, J. Phys.: Condens. Matter **2**, 1457 (1990).

[75] P.Giannozzi, S. de Gironcoli, P. Pavone, and S. Baroni, Phys. Rev. B **43**, 7231 (1991).

[76] N. W. Ashcroft and N. D. Mermin, *Solid State Physics* (W. B. Saunders Co., Orlando 1976).

[77] D. Powell, M. A. Migliorato, and A. G. Cullis, Physica E **32**, 270 (2006).

[78] M. Tang and S. Yip, Phys. Rev. B **52**, 15150 (1995).

[79] L. J. Porter, J. F. Justo, and S. Yip, J. Appl. Phys. **82**, 5378 (1997).

[80] C. Z. Wang, C. T. Chan, and K. M. Ho, Phys. Rev. B **42**, 11276 (1990).

[81] L. J. Porter, S. Yip, M. Yamaguchi, H. Kaburaki, and M. Tang, J. Appl. Phys. **81**, 96 (1997).

[82] H. J. C. Berendsen, J. P. M. Postma, W. F. van Gunsteren, A. DiNola, and J. R. Haak, J. Chem. Phys. **81**, 3684 (1984).

[83] Wolfram Research, Inc., Mathematica, Version 7.0, Champaign, IL (2008).

[84] A. P. Miller, in *Specific Heat of Solids*, edited by C. Y. Ho (Hemisphere Publishing Corp., New York, 1988).

[85] S. Adachi, in *Properties of Gallium Arsenide, 3rd ed.*, edited by M. R.Brozel and G. E.Stillman (INSPEC, London,1996).

[86] T. C. Cetas, C. R. Tilford, and C. A. Swenson, Phys. Rev. **174**, 853 (1968).

[87] U. Piesbergen, Z. Natforsch. **18**, 141 (1963).

[88] B. D. Lichter and P. Sommelet, Trans. Metall. Soc. AIME **245**, 1021 (1969).

[89] J. K. Blakemore, J. Appl. Phys. **53**, R123 (1982).

[90] V. M. Glazov and A. S. Pashinkin, Inorg. Mater. **36**, 225 (2000).

[91] P. Kratzer and M. Scheffler, Phys. Rev. Lett. **88**, 036102 (2002).

[92] K. Itagaki and K. Yamaguchi, Thermochim. Acta **163**, 1 (1990).

[93] L. Däweritz and R. Hey, Surf. Sci. **236**, 15 (1990).

[94] A. Kley, P. Ruggerone, and M. Scheffler, Phys. Rev. Lett. **79**, 5278 (1997).

[95] P. Kratzer, C. G. Morgan, and M. Scheffler, Prog. Surf. Sci. **59**, 135 (1998).

[96] M. A. Salmi, M. Alatalo, T. Ala-Nissila, and R. M. Nieminen, Surf. Sci. **425**, 31 (1999).